

Theoretical approach to photoinduced inhomogeneous anisotropy in bacteriorhodopsin films

P. Acebal, L. Carretero, S. Blaya, A. Murciano, and A. Fimia*

*Departamento de Ciencia y Tecnología de Materiales, Universidad Miguel Hernández,
Avenida Ferrocarril s/n Apartado Postal 03202 Edificio Torrevalillo, Elx (Alicante) Spain*

(Received 14 November 2006; published 30 July 2007)

The aim of this work was to perform a complete study of the dynamic and steady-state photoinduced processes of thick bacteriorhodopsin (bR) films, taking into account all the physical parameters and the coupling of rate equations with the energy transfer equation. The theoretical approach was compared with experimental data, and good concordance was found between both sets of data. The theoretical approach shows that the values of the rate constants for solid bR films are about two or three orders of magnitude lower than those observed in solution. It can also be noted that the temperature change during the experiment had a great influence on the final values of transmittance and, consequently, on the inhomogeneous distribution along the coordinate of light propagation. The study shows that, depending on the intensity and wavelength of the pump beam, we can obtain a very inhomogeneous profile of the population densities, which implies an inhomogeneous profile of the birefringence and dichroism. Therefore, this must be taken into account in the applications described for this system.

DOI: [10.1103/PhysRevE.76.016608](https://doi.org/10.1103/PhysRevE.76.016608)

PACS number(s): 42.70.-a, 78.20.Ci, 78.20.-e, 78.20.Bh

I. INTRODUCTION

The need for improved materials in many photonic applications has been the focus of much research activity in recent decades. Photochromic systems, whose optical properties change upon illumination, have been one of the most widely studied, since a great number of applications, such as optical memories [1] or all optical switching [2], has been described for them. The set of molecules that have photochromic properties can be divided into two categories according to their origin. On the one hand, we have the chemically engineered molecules [3,4], such as azo compounds or spirooxazine dyes, widely employed in the applications described above; the main problems with these were fatigue resistance and low switching speed in a rigid polymer matrix [5]. On the other hand, we have the biologically based materials, such as bacteriorhodopsin (bR) [6], which is contained within the purple membrane of members of the *haloarchaea* species. This last system has advantages over chemically engineered systems since it supports a large number of write-erasure cycles. Therefore, bR-containing materials have been used for many applications in optics, such as optical memories [6,7], optical phase conjugation [8], real-time holography [9–11], spatial light modulators [12,13], all optical switching [14], or holographic interferometry [15].

The main problem, or perhaps the main advantage, of the biological system bacteriorhodopsin is the number of states involved in the photocycle [6] (compared with the two states usually encountered in the chemically engineered systems), which makes it difficult to model the events that take place during the material's illumination, this being the usual procedure to improve the behavior of the material. There are many studies in the literature that describe the behavior of bacteriorhodopsin [16–21], but, due to the great complexity of the system, they usually use some approximations, which involve limitation of the number of bR states considered, or

decoupling of the radiative transfer equation (Beer's law) and the rate equations for the bR states. These approximations cause different problems, such as a lack of information about all the physical parameters of the system (rate constants or quantum efficiencies) in the first case and an incorrect description of the photoinduced inhomogeneity in the propagation direction of light in the second case.

The aim of this work was to perform a complete study of the dynamic and steady-state photoinduced processes of thick bacteriorhodopsin films, taking into account all the physical parameters and the coupling of rate equations with the energy transfer equation. The theoretical approach was compared with experimental data, which allowed us to validate the modelization procedure and to characterize some of the physical parameters of the bR in the film. These were different from those described in the literature [22,23], which are usually measured in solution. This study also allows us to characterize the anisotropy distribution along the film as a function of different experimental parameters, such as light intensity and wavelength or exposure time.

The bR films are composed of an inert matrix (usually a polymer or gelatin) and a large number of photochromic protein bacteriorhodopsin molecules. Regarding the description of the bR molecules, two different frames should be distinguished, depending on the optical properties. On the one hand, a chain of amino acids forms a helicoidal superstructure, whose main function is to serve as a rigid support for the light active core inside the bacterial membrane. This core is composed of a few amino acids and the retinal chromophore attached to the lysine 216 via protonated Schiff base linkage. The function of this active core is to act as a light-driven proton pump, transforming light energy into chemical energy by a mechanism that has been described previously [9,10], with a high quantum efficiency. This mechanism is composed of six states (see Fig. 1), starting from the *B* state, which upon illumination is converted into the *M* state via *K* and *L* states, and then returns to the *B* state via *N* and *O* states. Apart from the normal evolution of the photocycle, the protein can also return directly to the *B* state from *K*, *L*, *M*, and *N* states upon photon absorption. Another

*pablo@дите.umh.es

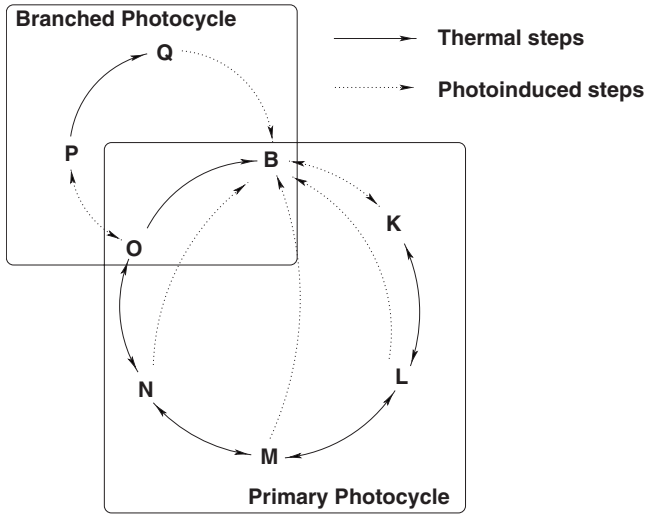


FIG. 1. Schematic representation of the bacteriorhodopsin photocycles.

photocycle was discovered in bR by Popp *et al.* [24]. This second photocycle is coupled with the first one, since it starts at the *O* state, which upon photon absorption is converted into the *P* state. The evolution of the *P* state is described in detail in Ref. [25]. Basically, two transitions are possible for the *P* state: it could return to the *O* state upon illumination with green light (absorption maximum around 525 nm), or it could be converted into the *Q* state due to thermal decay. Upon photon absorption, the *Q* state returns to the *B* state and closes the photocycle. It is important to note that *Q* and *P* states are thermally stable [25] (they only return to the primary photocycle upon illumination), so they are important for certain photonic applications like optical data storage [26].

II. THEORETICAL BACKGROUND

In order to describe the photoinduced changes in a photochromic material, the intensity distribution along the film must be known. Therefore, the starting point is the equation for radiative energy transfer along an inhomogeneous medium:

$$\frac{\partial I_a(\zeta, t)}{\partial \zeta} = -[\beta_{aa}(\zeta, t) + \beta_{aa}^R(\zeta, t)]I_a(\zeta, t), \quad (1)$$

where I_a is the intensity of the pump beam polarized along the a direction, ζ is the propagation coordinate of the electromagnetic field, and β_{aa} and β_{aa}^R are the macroscopic magnitudes related to the microscopic absorption and scattering cross sections. We only consider the existence of an electric field polarized along the a direction, so the model described is valid for initially isotropic systems (the most usual case) and when the a direction is one of the main axes for an anisotropic film. For a system formed by N^κ classical bodies in the κ state ($\kappa \in \{B, K, L, M, N, O, P, Q\}$), statistical mechanics can be applied to obtain the expressions of these macroscopic magnitudes as a function of the corresponding microscopic properties:

$$\beta_{aa}(\omega, \zeta, t) = \sum_{\forall \kappa} \sum_i^3 N_{ia}^\kappa(\zeta, t) \sigma_{ii}^\kappa(\omega), \quad (2)$$

$$\beta_{aa}^R(\omega, \zeta, t) = \sum_{\forall \kappa} \sum_i^3 N_{ia}^\kappa(\zeta, t) \sigma_{ii,R}^\kappa(\omega) + \sum_i^3 N_{ia}^m \sigma_{ii,R}^m, \quad (3)$$

where σ_{ii}^κ and $\sigma_{ii,R}^\kappa$ are the components of the microscopic absorption and scattering cross section matrices of the κ state of bR, respectively, and $\sigma_{ii,R}^m$ denotes the microscopic scattering cross section of the matrix, N_{ia}^κ are the population densities of bacteriorhodopsin units in the κ state with the i component of the cross section projected along the a coordinate of the macroscopic frame, and N_{ia}^m is the density of molecules of the inert matrix. Therefore, we need to know the time evolution of the population densities of bacteriorhodopsin units for each state to solve the time evolution of the transmitted intensity. This time evolution is given by the rate equation system for the population densities, which can be written in matrix form as

$$\mathbf{B} = \mathbf{A} \cdot \mathbf{n}_{ia}, \quad (4)$$

where the \mathbf{B} and \mathbf{n}_{ia} vectors are $\mathbf{B} = \{\partial n_{ia}^B / \partial t, \partial n_{ia}^K / \partial t, \partial n_{ia}^L / \partial t, \partial n_{ia}^M / \partial t, \partial n_{ia}^N / \partial t, \partial n_{ia}^O / \partial t, \partial n_{ia}^P / \partial t, \partial n_{ia}^Q / \partial t, 1\}$ and $\mathbf{n}_{ia} = \{n_{ia}^B, n_{ia}^K, n_{ia}^L, n_{ia}^M, n_{ia}^N, n_{ia}^O, n_{ia}^P, n_{ia}^Q\}$, while the coefficient matrix \mathbf{A} is

$$\mathbf{A} = \begin{pmatrix} -\Phi_{ia}^B & \Phi_{ia}^K & \Phi_{ia}^L & \Phi_{ia}^M & \Phi_{ia}^N & k_{ob} & 0 & \Phi_{ia}^Q \\ \Phi_{ia}^B & -k_K & k_{lk} & 0 & 0 & 0 & 0 & 0 \\ 0 & k_{kl} & -k_L & k_{ml} & 0 & 0 & 0 & 0 \\ 0 & 0 & k_{lm} & -k_M & k_{nm} & 0 & 0 & 0 \\ 0 & 0 & 0 & k_{mn} & -k_N & k_{on} & 0 & 0 \\ 0 & 0 & 0 & 0 & k_{no} & -k_O & \Phi_{ia}^P & 0 \\ 0 & 0 & 0 & 0 & 0 & \Phi_{ia}^O & -k_P & 0 \\ 1 & 1 & 1 & 1 & 1 & 1 & 1 & 1 \end{pmatrix}, \quad (5)$$

where the k_κ coefficients are

$$k_K = \Phi_{ia}^K + k_{kl}, \quad (6)$$

$$k_L = \Phi_{ia}^L + k_{lk} + k_{lm}, \quad (7)$$

$$k_M = \Phi_{ia}^M + k_{ml} + k_{mn}, \quad (8)$$

$$k_N = \Phi_{ia}^N + k_{nm} + k_{no}, \quad (9)$$

$$k_O = \Phi_{ia}^O + k_{ob} + k_{on}, \quad (10)$$

$$k_P = \Phi_{ia}^P + k_{pq}, \quad (11)$$

and the terms Φ_{ia}^κ are given by

$$\Phi_{ia}^\kappa = \frac{\phi_\kappa}{\hbar\omega} \sigma_{it}^\kappa I_a. \quad (12)$$

In this system, n_{ia}^κ are the normalized population densities for the κ state ($n_{ia}^\kappa = N_{ia}^\kappa / N_{ia}^{bR}$), the parameters ϕ_κ are the quantum efficiencies of the photoinduced reactions, and $k_{\kappa\kappa'}$ are the rate constants of the transition $\kappa \rightarrow \kappa'$ (we have omitted the dependency on ζ and time of all the population densities and the light intensity of the pump beam for simplicity). Also, it should be noted that the equations may be simplified, depending on the pump beam wavelength; for example, for a working wavelength of 532 nm the M and the O states do not absorb ($\Phi_{ia}^M = \Phi_{ia}^O = 0$). The last line of the coefficient matrix accounts for the conservation of the total purple membrane units oriented in a fixed direction ($N_{ia}^{bR} = N_T/3$ for isotropic nonoriented films). This conservation can be assumed for bacteriorhodopsin chromophores contained in a rigid solid matrix (without free rotation of the purple membrane units) due to the rigidity of the light active core [27] (in other photochromic systems this cannot be assumed, because the isomerization is independent of the initial direction [28]). It is important to note that, for other material configurations, such as dense solutions of bR, the model would be modified, in order to take into account the rotation effect. In that case, the modifications would include new free parameters (rotation diffusion constants), and an increase in the number of unknown functions. Therefore, the system becomes extremely complex, with a solution vector of 24 components and a coefficient matrix \mathbf{A} of 24×24 elements.

At this point we have a set of equations that describe photoinduced processes in thick bR films, which has seven unknown functions (the six bR state population densities and the pump intensity), a large number of parameters (rate constants, quantum efficiencies, and microscopic optical properties), and two variables (position and time). This system has no analytical solutions for time and position, and therefore we have to employ numerical methods. In the next section, we proceed to define the different parameters of the systems, which we divide into two categories according to the effect of the environment.

A. Rate constants and quantum efficiencies

The first set of parameters are the rate constants and quantum efficiencies of the different transitions of the photocycle. This set is characterized by the large influence of the environment on the values, due to the transmembrane nature of BR, mainly the water content and the pH; however, chemical additives [13,29] in the polymer matrix also have a dramatic influence on the rate constants. In the case of the rate constants, it is also important to note that their values depend on the temperature, which is not constant during the pump stage, so it has to be taken into account. The temperature dependency of the rate constants is given by the Eyring relationship [30], which allows us to represent the rate constant at a given temperature T_1 as a function of the k_0 at another temperature T_0 :

$$k_1 = \frac{k_B T_1}{h} \left(\frac{h k_0}{k_B T_0} \right)^{T_0/T_1}, \quad (13)$$

where k_B and h are the Boltzmann and Planck constants, respectively. A rigorous treatment of the temperature change during the experiment involves the use of the heat transfer equation, which in principle is a three-dimensional equation, coupled with all the equations present in the paper with a complex dependency. Also, new free parameters will be introduced, such as the heat capacity and thermal conductivity. In order to simplify, we use an approximation of the temperature function, which is based on two reasonable arguments: (i) the temperature change is an equilibrium between the increase due to light absorption and decrease due to thermal dissipation, which occurs with different time constants; (ii) the maximum temperature is not higher than 340 K for light intensities of about 2000–3000 W/m², since no degradation of the protein is observed in the experiments at these intensities. Making these assumptions, we can represent the temperature function during the experiment as

$$T = T_0 + a_{in} \left(1 - \sum_i b_i e^{-c_i t} \right) - a_{de} \left(1 - \sum_i h_i e^{-g_i t} \right), \quad (14)$$

where the coefficients a_{in} and a_{de} account for the total temperature increase due to light absorption and decrease due to thermal dissipation, respectively, and both depend on the incident intensity. The temporal behavior is described as a combination of ascending saturation curves for the heating process and descending saturation curves for the dissipation process, where c_i and g_i are the time constants of these processes, weighted with the coefficients b_i and h_i ($\sum_i b_i = 1$ and $\sum_i h_i = 1$).

Numerical values of all these parameters in the bR film cannot be easily determined with any experimental technique, so they were free parameters in the fitting procedure of experimental curves. Since they are intrinsic properties of the material, it is important to note that the same values at a given temperature will explain the experimental data in different conditions (such as different incident intensities).

B. Microscopic optical properties

The second set of parameters that we have in the equations are the microscopic optical properties of all the ele-

TABLE I. Values for the microscopic optical properties of the different states of bR (μ_{1g} and λ_{1g} from Refs. [26,33]).

	<i>B</i>	<i>K</i>	<i>L</i>	<i>M</i>	<i>N</i>	<i>O</i>	<i>P</i>	<i>Q</i>
$\alpha_{xx}^C(0)$ (10^{-28} m ³)	20.46		26.25	12.88		21.78		
$\alpha_{yy}^C(0)$ (10^{-28} m ³)	5.87		10.33	5.59		5.67		
$\alpha_{zz}^C(0)$ (10^{-28} m ³)	4.35		4.35	3.78		4.19		
$\mu_{1g,x}$ (10^{-29} C m)	3.75	3.38	3.17	2.95	2.65	3.95	3.36	2.79
λ_{1g} (10^{-9} m)	560	610	548	410	560	640	525	390

ments of the system, which are not affected by the environment (*pH* and water content). Concretely, we need the values of the microscopic absorption cross sections of the different states of the system and the microscopic scattering cross sections for the working wavelength, which are given by [31,32]

$$\sigma_{ii}^{\kappa}(\omega) = \frac{\omega(\mu_{eg,i}^{\kappa})^2 \exp[-(\omega - \omega_{eg}^{\kappa})^2/2\gamma^2]}{c\hbar\epsilon_0 \sqrt{2\pi\gamma}}, \quad (15)$$

$$\sigma_{ii,R}^{\kappa}(\omega) = \frac{24\pi[\alpha_{ii}^{\kappa}(\omega)]^2\omega^4}{9c^4}, \quad (16)$$

where μ_{eg}^{κ} is the ground to excited state transition dipole moment of the κ state of bR, ω_{eg}^{κ} ($\omega_{eg}^{\kappa} = 2\pi c/\lambda_{eg}^{\kappa}$) is the frequency of this transition, γ denotes the width of the absorption curve, $\alpha_{ii}^{\kappa}(\omega)$ is the polarizability of the κ element at ω , c is the light speed, and ϵ_0 is the dielectric permittivity of the vacuum. In order to assign reliable numerical values to these microscopic parameters, we follow two different strategies. On the one hand, we use experimental values present in the literature for μ_{eg}^{κ} , ω_{eg}^{κ} , and γ [26,33], which allow us to have a complete description of the absorption cross section of the system. On the other hand, we have the polarizability components, which cannot be easily measured experimentally, so we evaluate these components using quantum mechanical simulations with a procedure described in a previous study [34] for two states of the system (all the calculations were performed with the GAUSSIAN 98 package [35]). In this previous work, we considered that the polarizability of the different states of the bacteriorhodopsin can be separated into the contribution of the light active core and that of the structural chain of amino acids (α_0 , $\hat{\alpha}^{C\kappa}$):

$$\hat{\alpha}^{\kappa} = \alpha_0 \hat{I} + \hat{\alpha}^{C\kappa}, \quad (17)$$

where α_0 denotes the sum of the traces of static polarizability of the 296 amino acids that form the bR protein, and $\hat{\alpha}^{C\kappa}$ is the polarizability matrix of the light active core of the protein (retinal chromophore and surrounding amino acids). The elements of the polarizability matrix are given by the equation

$$\alpha_{ii}^{C\kappa}(\omega) \approx \sum_{e,e \neq 1} \alpha_{ii,e}^{C\kappa}(0) + \alpha_{ii,1}^{C\kappa}(0) \Omega_1^{C\kappa}(\omega; \omega), \quad (18)$$

where $\alpha_{ii,e}^{C\kappa}(0)$ and $\Omega_1^{\kappa}(\omega)$ are

$$\alpha_{ii,e}^{C\kappa}(0) = \frac{2(\mu_{eg,i}^{\kappa})^2}{\hbar\epsilon_0\omega_{eg}^{\kappa}}, \quad (19)$$

$$\Omega_1^{C\kappa}(\omega; \omega) = \frac{(\omega_{1g}^{\kappa})^2 [(\omega_{1g}^{\kappa})^2 - \omega^2]}{[(\omega_{1g}^{\kappa})^2 - \omega^2]^2 + \Gamma^2 \omega^2}. \quad (20)$$

Here Γ is the damping factor, related to the width of the absorption curve. The values of the microscopic optical properties of the different states of bR are shown in Table I, with the other values used being $\gamma = \Gamma/2.355 = 2 \times 10^{14}$ s⁻¹ and $\alpha_0 = 2.76 \times 10^{-26}$ m³. The polarizabilities of *K*, *N*, *P*, and *Q* states of bR were not calculated, since their population densities were two orders of magnitude lower than those of the other states, so their contribution to the scattering losses was negligible in this study.

III. MODELIZATION PROCEDURE

In the modelization procedure, we distinguish two different cases, the steady state and the time-dependent response. In both cases, the problem described has no analytical solutions, so numerical treatment was required. However, the way to solve the problem was different in each case. For the steady-state case, all the time derivatives of the population densities are equal to 0, so the **B** matrix is now $\mathbf{B}^{\infty} = \{0, 0, 0, 0, 0, 0, 0, 1\}$, which implies that we have a system of linear equations for the population densities, with the following solution:

$$\mathbf{n}_{ia}^{\infty}(I_a(\xi)) = \mathbf{A}^{-1} \cdot \mathbf{B}^{\infty} \quad (21)$$

where \mathbf{A}^{-1} is the inverse of the coefficient matrix and ∞ indicates the steady state (infinity time). This solution gives us an analytic expression for the population densities as a function of the different parameters of the system and the light intensity function, which now depends only on the coordinate of the propagation direction. Therefore, the expressions for the population densities were introduced in Eq. (1), resulting in a differential equation with one unknown function and one variable:

$$\frac{dI_a(\xi)}{d\xi} = - \left(\sum_{\forall \kappa} \sum_i^3 N_{ia}^{bR} n_{ia}^{\kappa, \infty} [\sigma_{ii}^{\kappa}(\omega) + \sigma_{ii,R}^{\kappa}(\omega)] + \sum_i^3 N_{ia}^m \sigma_{ii,R}^m \right) I_a(\xi). \quad (22)$$

This equation was solved with standard numerical methods. Then the intensity function was introduced in the population density expressions to find their distribution along the propagation direction (inhomogeneous distribution).

The way to solve the time-dependent case was different, since for this case we had a set of coupled differential equations that depends on two variables, and the numerical approach was also a difficult task. We solve the system by decoupling the differential equation for the ζ variable from those for the time variable, which can be done if we discretize the material in the light propagation direction. For an adequate number of layers [or step size ($\Delta\zeta$)], we considered that the population densities do not depend on the ζ variable, so Eq. (1) can be solved analytically for each layer, and the transmitted intensity of the j layer is

$$I_a[j] = I_a[j-1] \exp \left[- \left(\sum_{\kappa} \sum_i^3 N_{ia}^{\kappa}(j,t) [\sigma_{ii}^{\kappa}(\omega) + \sigma_{ii,R}^{\kappa}(\omega)] + \sum_i^3 N_{ia}^m \sigma_{ii,R}^m \right) \Delta\zeta \right], \quad (23)$$

where the $N_{ia}^{\kappa}(j,t)$ were solved with the rate equations (which depend only on the time variable), taking into account that the intensity function needed to solve the j layer was that of the $j-1$ layer.

IV. EXPERIMENTAL PROCEDURE

The theoretical model was evaluated with experimental data obtained with a standard setup for a commercially available bacteriorhodopsin film (MIB), whose main characteristics were an optical density of 2.8 at 560 nm and a thickness of 100 μm . For the experimental setup, we used a linearly polarized pump beam from a frequency-doubled Nd:VO₄ laser operating at 532 nm. This beam was expanded, collimated, and limited to an area as small as possible, to ensure a homogeneous distribution of the light intensity (center of the Gaussian distribution). The signal was monitored in real time using a photodetector positioned behind the sample. The experiment was repeated at 11 different intensities of the pump beam.

V. RESULTS AND DISCUSSION

First, we must assign reliable values to the rate constants and quantum efficiencies. As mentioned above, this was done by fitting experimental values with the model, where the rate constants and quantum efficiencies were free parameters. It is important to note that, as a consequence of the experimental conditions [in particular, of the pump beam wavelength (532 nm), $\Phi_{ia}^M \approx 0$ and $\Phi_{ia}^O \approx 0$ due to the low absorption of the M and O states], ϕ_M and all the parameters related to the branched photocycle (ϕ_O , ϕ_P , ϕ_Q , and k_{pq}) could not be determined. Therefore, the discussion of the inhomogeneous distribution of the population densities is valid for a range of the pump beam wavelength between 500 and 560 nm, approximately, which is the wavelength usually employed for applications like all optical switching or spatial light modulators. An analysis of the influence of the branched photocycle of the bR would involve the study of the transmittance curves with a pump beam frequency near the absorption maximum of the O state, for which Φ_{ia}^O

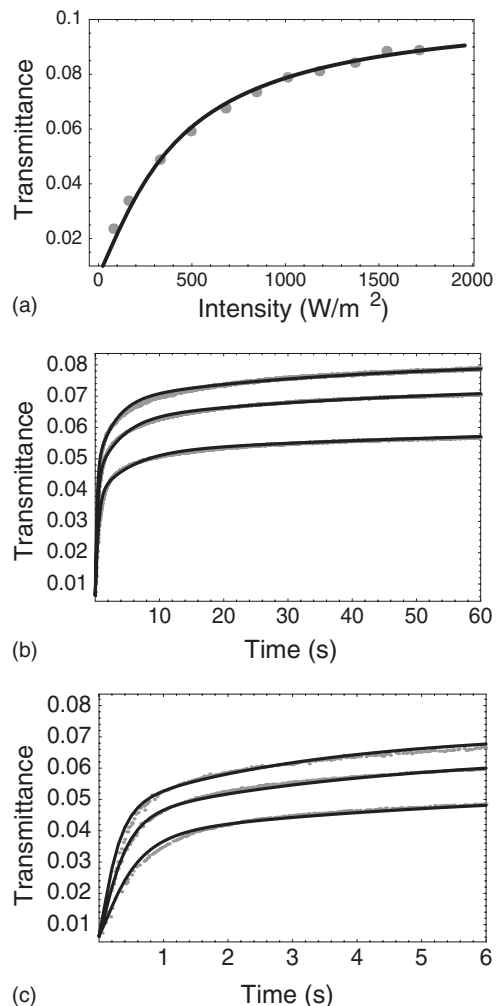


FIG. 2. (a) Theoretical (black lines) and experimental (gray points) results for the transmittance at the steady state for different incident intensities. (b), (c) Theoretical and experimental results for the transmittance dynamic response (calculations done with 100 layers) for three different incident intensities (514, 844, and 1180 W/m²).

$> \Phi_{ia}^P$, so the population densities of the P and Q states will be appreciable. This will be important for applications where the photoinduced changes remain a long time after the pump stage; however, this aspect was outside the scope of this study.

The results of the fitting procedure are shown in Fig. 2, where we present two different sets of experimental results (steady-state and time-dependent responses). First, we fitted the steady-state data, which gave us a set of values for the parameters $\{k_{kl}, \dots, \phi_B, \dots\}$, whose main characteristic is that if we multiply all the values by a constant ξ , then these new values also fit the experimental result. Therefore, to obtain a unique solution for the parameters we fitted the dynamic data, where now we had only one free parameter (ξ). This procedure showed that we cannot assign reliable values to the physical parameters of the system with steady-state data only. It is important to note that the numerical treatment employed makes it difficult to demonstrate the uniqueness of the fitting, since we do not have an analytical expression to

fit, and therefore expressions for the gradient and the Hessian were not available. The fitting procedure involves the calculation of the regression coefficient for a large number of sets of values for the parameters. First, a large step size is used, which allows us to assign an order of magnitude for each parameter, and later a more accurate step size is employed to obtain the best-fit parameters. We try to ensure the uniqueness of the fitting using the steady state and three dynamic response curves, since we think that it is possible to have two different sets of parameters that fit the steady state and one dynamic response curve with relatively good concordance. However, it is difficult for these different sets to fit three dynamic responses correctly, since these responses depend nonlinearly on the parameters.

As can be seen, good concordance (regression coefficients higher than 0.97) was found between both sets of data using the following values of rate constants and ϕ_K at 293 K (ambient temperature): $k_{kl}=2300$ (± 200) s^{-1} , $k_{lm}=169$ (± 2) s^{-1} , $k_{mn}=0.98$ (± 0.05) s^{-1} , $k_{no}=110$ (± 10) s^{-1} , $k_{ob}=5.2$ (± 0.3) s^{-1} , $k_{jk}=230$ (± 20) s^{-1} , $k_{ml}=64.6$ (± 0.6) s^{-1} , $k_{nm}=40$ (± 4) s^{-1} , $k_{on}=0.1$ (< 1) s^{-1} , $\phi_B=0.12$ (± 0.001), $\phi_K=0.12$ (< 0.2), $\phi_L=0.12$ (± 0.001), and $\phi_N=0.8$ (> 0.6). The values in parentheses mark the confidence interval for the parameters, based on the change in the regression coefficients when we modify the values of each parameter. It can be seen that the width of the confidence interval changes from one parameter to the other. All of them were relatively narrow, except three related to the N and K states, for which the interval was broad. This may be attributed to the low values of the population densities for the N and K states, and has no effect on the calculation of the inhomogeneous distribution of the anisotropy. Other free parameters of the model were the coefficients of the temperature function [Eq. (14)], which were $a_{in}=0.47\sqrt{I_a(0)}$, $a_{de}=0.6a_{in}$, $b_1=1$, $h_1=0.6$, $h_2=0.4$, $c_1=10$, $g_1=0.02a_{in}$, and $g_2=0.0014a_{in}$. These temperature parameters basically mean that there was a rapid increase in the temperature due to the absorption (which depends on the incident intensity), and later a slow decrease in the temperature due to the equilibrium between absorption and dissipation, where the rate constants of the decrease depend on the temperature reached. Using these parameters, the temperature change is about 8 K for the steady state and the highest intensity employed (2000 W/m^2), so the approximation that disregards the temperature gradient seems correct. We test this approximation experimentally using two diaphragms, one before and one after the film. In the standard setup both have the same radius, while, in the second experimental setup, the first diaphragm is open with the largest radius, so we changed the temperature gradient in the xy plane. Since both transmittance curves are similar, we considered that the effect of the temperature gradient was negligible.

Figure 2(a) shows the transmittance [defined as $I_a(L,t)/I_a(0,t)$] of the pump beam at the steady state, using different values of the incident intensity, for both experimental and theoretical data. The observed and calculated curves show the typical saturation form for photochromic systems, where saturation was found for an intensity slightly higher than 2000 W/m^2 . These values of the parameters also reproduce the dynamic behavior of the transmittance, as can be

seen in Figs. 2(b) and 2(c), where the dynamic response for the three different incident intensities (514, 844, and 1180 W/m^2) is shown. Figures 2(b) and 2(c) are the same but with different time scales, which shows the good concordance between experimental and theoretical data for short and long times. It is important to note that the experimental results for short times (0–2 s) can be reproduced without the temperature effect on the rate constants using different values from those shown before, but this model does not allow us to reproduce the dynamic response for long times. Therefore, the observed evolution of the transmittance after the first change in the slope (between 1 and 2 s depending on the incident intensity) must be attributed to the change in temperature during the experiment. Regarding the values of the rate constants which reproduce the steady-state and dynamic behavior of bR films, it should be noted that they were between two and three orders of magnitude lower than those reported in the literature [22,23], which were measured in solution. These results must be mainly due to the effect of the water content, since, as mentioned above, the values of the rate constants are greatly modified by this parameter [15], and it is obvious that the water concentration in a solution is quite different from that in a solid film. The other parameters that modify the rate constants— pH and chemical additives—could be similar for a solution and for a solid matrix, so the main effect must be due to the water content.

The good concordance between theoretical and experimental data confirms that the model was a good approximation of the events that take place during illumination of the material, so we could use all the information obtained to find out more about what occurs inside the material. In particular, we were interested in the inhomogeneous distribution of the normalized population densities along the light propagation direction. This is an important parameter needed to analyze the photoinduced anisotropy, which can be defined as the difference between the population densities with the x component of the microscopic frame projected along the a and b coordinates of the macroscopic frame:

$$\Delta n_x^K = n_{xa}^K - n_{xb}^K. \quad (24)$$

The n_{xa}^K depends on the coordinate of the propagation direction, and n_{xb}^K is constant for the systems studied here, so Eq. (24) implies that the anisotropy depends on the coordinate of the propagation direction with the same dependency as n_{xa}^K . Therefore, the study of the inhomogeneous profile for the population densities also shows the inhomogeneous distribution of the material anisotropy. Therefore, birefringence and dichroism (a lot of applications are based on these properties) vary with the depth of the sample. The study of the inhomogeneous distribution was done for both cases, steady state and time dependency. Simulations for the steady state are shown in Fig. 3. First, in Fig. 3(a), we analyze the effect of the light intensity. The behavior of the curve is as expected, since the results showed that the population of the initial B state increases with depth as a result of the attenuation of the pump beam intensity, while the population of the

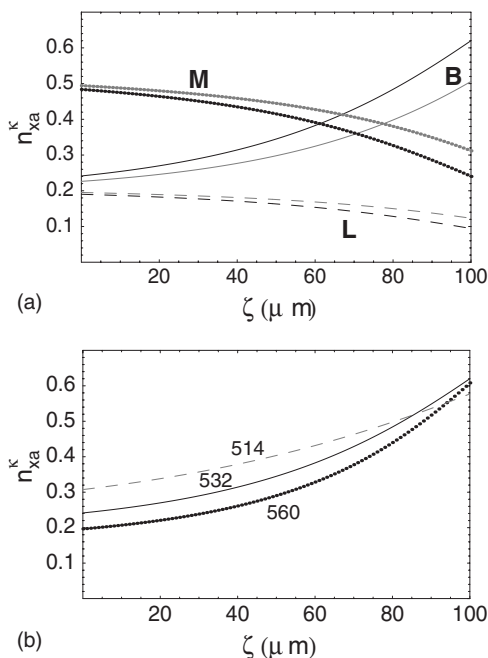


FIG. 3. (a) Normalized population densities (n_{xa}) of different states of bR versus the coordinate of light propagation for two incident intensities (black, 514 W/m^2 ; gray, 1180 W/m^2). (b) Normalized population density (n_{xa}) of B state of bR versus the coordinate of light propagation for three different wavelengths of the pump beam at 514 W/m^2 .

other states decreases. Another expected result was the fact that the increase in the incident intensity causes a smaller difference between the population densities of the first and the last layers, where, for example, at 1180 W/m^2 , the population density of the L state was close to a homogeneous distribution. This was not the case for the B and M states, for which higher intensities are needed. The change in n_{xa}^kappa with increase in the intensity of the pump beam is greater for the last layers, since for the first layers saturation was reached. An interesting result is also shown in Fig. 3(b), where we analyze the effect of the wavelength of the pump beam on the photoinduced anisotropy. The difference between initial and final layers was greater for the pump wavelength near the resonance of the B state (560 nm) with the same intensities, while a more homogeneous result is obtained with a wavelength outside resonance (514 nm). Regarding the values of the initial layer, it should also be commented that the photoconversion efficiency reached, defined as $1 - n_{xa}^B$, was higher for a wavelength near resonance, so higher anisotropies could be obtained using this wavelength.

Finally, we analyze the dynamic behavior of the photoinduced inhomogeneous anisotropy. Figure 4(a) shows the evolution of the normalized population densities of the B and M states of bR with the depth of the sample for different times. We can distinguish two different time scales for the profile change during the pump state, one for an interval between 0 and 2 s, where the greatest change in the form of the profile is produced, and the other for a time longer than 2 s. As mentioned above, the results for the first interval can be explained basically by the values of the different rate constants

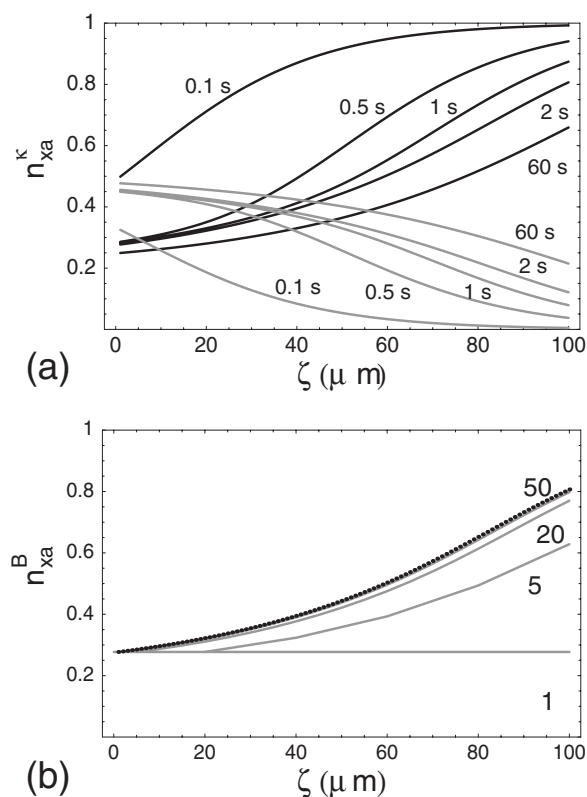


FIG. 4. (a) Normalized population densities (n_{xa}) of the B (black) and M (gray) states of bR versus the coordinate of light propagation for five different times with an intensity of 514 W/m^2 . (b) Normalized population density (n_{xa}) of the B state of bR versus the coordinate of light propagation for five different step sizes (1, 5, 20, 50, and 100 layers) at 2 s with an intensity of 514 W/m^2 (points indicate the results for 100 layers).

without the influence of the temperature (to be more precise, we can say that the temperature influence is not remarkable at this stage). After this time, the form of the profile does not change significantly, and we only observe a decrease in the whole curve for n_{xa}^B and an increase for n_{xa}^M until the steady state is reached, which happens at long times (more than 100 s). Figure 4(b) analyzes the importance of a correct selection of the step size in the modelization procedure of the time response. As can be seen, the results converged for values of step size greater than $2 \mu\text{m}$ (50 layers), whereas when we used a smaller number of layers we could not reproduce the inhomogeneous distribution correctly.

VI. CONCLUSIONS

We performed a complete study of the dynamic and steady-state photoinduced processes of thick bacteriorhodopsin films, taking into account all the physical parameters and the coupling of rate equations with the energy transfer equation, and obtained good concordance between theoretical and experimental data. The theoretical approach shows that the values of the rate constants of the primary photocycle for solid bR films are about two or three orders of magnitude

lower than those observed in solution. It can also be noted that the temperature change during the experiment had a great influence on the final values of transmittance and, consequently, on the inhomogeneous distribution along the coordinate of light propagation. The study shows that, depending on the intensity and wavelength of the pump beam, we can obtain a very inhomogeneous profile of the population densities, which implies an inhomogeneous profile of the bi-

refringence and dichroism. Therefore, this must be taken into account in the applications described for this system.

ACKNOWLEDGMENTS

The authors acknowledge support from Projects No. MAT2004-04643-C03-03 and No. FIS2006-09319 of Ministerio de Ciencia y Tecnología of Spain.

-
- [1] W. Tomlinson, *Appl. Opt.* **23**, 3990 (1984).
 [2] T. Ikeda and O. Tsutsumi, *Science* **268**, 1873 (1995).
 [3] J. Delaire and K. Nakatani, *Chem. Rev. (Washington, D.C.)* **100**, 1817 (2000).
 [4] G. Berkovic, V. Krongauz, and V. Weiss, *Chem. Rev. (Washington, D.C.)* **100**, 1741 (2000).
 [5] R. Evans, T. Hanley, M. Skidmore, T. Davis, G. Such, L. Yee, G. Ball, and D. Lewis, *Nat. Mater.* **4**, 249 (2005).
 [6] R. R. Birge, *Annu. Rev. Phys. Chem.* **41**, 683 (1990).
 [7] N. Hampp, *Chem. Rev. (Washington, D.C.)* **100**, 1755 (2000).
 [8] O. Werner, B. Fischer, A. Lewis, and I. Nebenzahl, *Opt. Lett.* **15**, 1117 (1990).
 [9] N. Hampp, A. Popp, C. Bruchle, and D. Oesterhelt, *J. Phys. Chem.* **96**, 4679 (1992).
 [10] J. D. Downie and D. T. Smithey, *Appl. Opt.* **35**, 5780 (1996).
 [11] A. Fimia, P. Acebal, A. Murciano, S. Blaya, L. Carretero, M. Ulibarrena, R. Aleman, M. Gomariz, and I. Meseguer, *Opt. Express* **11**, 3438 (2003).
 [12] R. Thoma, N. Hampp, C. Bruchle, and D. Oesterhelt, *Opt. Lett.* **16**, 651 (1991).
 [13] Q. W. Song, C. Zhang, R. Blumer, R. B. Gross, Z. Chen, and R. Birge, *Opt. Lett.* **18**, 1373 (1993).
 [14] P. Wu, D. Rao, B. Kimball, M. Nakashima, and B. DeCristofano, *Appl. Phys. Lett.* **81**, 3888 (2002).
 [15] A. Seitz and N. Hampp, *J. Phys. Chem. B* **104**, 7183 (2000).
 [16] D. Timucin and J. Downie, *J. Opt. Soc. Am. B* **12**, 3285 (1997).
 [17] D. Timucin and J. Downie, *J. Opt. Soc. Am. B* **17**, 202 (2000).
 [18] E. Korchemskaya, D. Stepanchikov, A. Druzko, and T. D. TV, *J. Biol. Phys.* **24**, 201 (1999).
 [19] C. Singh and S. Roy, *Optik (Stuttgart)* **113**, 373 (2002).
 [20] G. Hegde and K. Reddy, *Curr. Sci.* **85**, 1587 (2003).
 [21] R. Banyal, G. Hegde, B. Prasad, and K. Reddy, *Curr. Appl. Phys.* **5**, 133 (2005).
 [22] K. Ludmann, C. Gergely, and G. Varo, *Biophys. J.* **75**, 3110 (1998).
 [23] I. H. M. van Stokkum and R. L. Lozier, *J. Phys. Chem. B* **106**, 3477 (2002).
 [24] A. Popp, M. Wolperdinger, N. Hampp, C. Brauchle, and D. Oesterhelt, *Biophys. J.* **65**, 1449 (1993).
 [25] N. Gillespie *et al.*, *J. Phys. Chem. B* **106**, 13352 (2002).
 [26] J. A. Stuart, D. L. Marcy, K. J. Wise, and R. R. Birge, *Synth. Met.* **127**, 3 (2002).
 [27] B. Borucki, H. Otto, and M. Heyn, *J. Phys. Chem. B* **103**, 6371 (1999).
 [28] T. Pedersen, P. Johansen, N. Holme, P. Ramanujam, and S. Hvilsted, *J. Opt. Soc. Am. B* **15**, 1120 (1998).
 [29] E. Korchemskaya, D. Stepanchikov, and T. Dyukova, *Opt. Mater.* **14**, 185 (2000).
 [30] H. Eyring, *Chem. Rev. (Washington, D.C.)* **17**, 65 (1935).
 [31] V. May and O. Khn, *Charge and Energy Transfer Dynamics in Molecular System* (Wiley-VCH, Berlin, 2000).
 [32] C. Penney, *J. Opt. Soc. Am.* **59**, 34 (1969).
 [33] J. Y. Huang, Z. Chen, and A. Lewis, *J. Phys. Chem.* **93**, 3314 (1989).
 [34] P. Acebal, S. Blaya, L. Carretero, and A. Fimia, *Phys. Rev. E* **72**, 011909 (2005).
 [35] M. J. Frisch *et al.*, *GAUSSIAN 98*, Revision A.7 (Gaussian, Inc., Pittsburgh, PA, 1998).